

Variations of Mars gravitational field based on the NASA/Ames general circulation model

Braulio V. Sanchez,¹ D. D. Rowlands,² and Robert M. Haberle³

Received 7 April 2005; revised 20 December 2005; accepted 6 January 2006; published 21 June 2006.

[1] The NASA/Ames general circulation model (GCM) has been used to compute time series for the variations in the Stokes coefficients expressing Mars' gravitational field in spherical harmonics. The sources of the variations are changes in the mass distribution of the atmosphere and changes in the planetary ice caps. The latter are due mainly to the condensation and sublimation of CO₂ on the surface of Mars. Variations were obtained for coefficients up to degree and order 40, which is the maximum allowed by the spatial definition of the model. The time series covered a period of a full Martian year of 669 sols with a time step of 1.5 hours. The time series were analyzed by means of fast Fourier transforms. The largest variations occur in C₁₀ corresponding to a 27.5-mm displacement of the center of mass in the z-direction. Other geoidal variations are C₃₀ (17.7 mm), C₂₀ (11.4 mm) and C₅₀ (10.0 mm). The main harmonics are annual, (1/2)-annual and (1/3)-annual. Most of the power is due to ice caps variations. Mars Global Surveyor trajectory runs with and without the above orbit perturbations yield RMS differences in total position which range between 4.44 and 17.39 m over a 7-day arc, depending on the season. A 7-day simulated tracking data least squares solution in which some level of the perturbations is absorbed into initial state parameters yields RMS differences between 0.35 and 0.78 m in total position.

Citation: Sanchez, B. V., D. D. Rowlands, and R. M. Haberle (2006), Variations of Mars gravitational field based on the NASA/Ames general circulation model, *J. Geophys. Res.*, *111*, E06010, doi:10.1029/2005JE002442.

1. Introduction

[2] Mars' atmospheric CO₂ cycle and the associated waxing and waning of the polar caps are well known [i.e., Kieffer *et al.*, 1992; Hartmann, 1993]. Recent high-resolution images from the Global Surveyor and thermal images from Mars Odyssey suggest that the difference between the two poles is that the south pole dry-ice cover is thicker and does not disappear entirely during the summertime [Byrne and Ingersoll, 2003].

[3] The north-south differences stem from several causes. One of them is Mars high orbital eccentricity and the times of occurrences of apoapsis and periapsis: The largest variation in polar cap radial extension corresponds to the Southern Hemisphere in which summer coincides with perihelion and winter coincides with aphelion. The opposite is true for the Northern Hemisphere, where the polar cap variation is smaller. Another factor is the difference in polar elevation [Smith *et al.*, 1999]: The geopotential elevation of the south pole is 6 km higher than the north pole, resulting in lower pressures and temperatures in the south. Finally,

the north polar cap has a lower albedo than the southern one, resulting in a more effective sublimation of CO₂. Another consequence of Mars higher insolation in the Southern Hemisphere is the creation of dust storms which originate in the south in late spring but grow to global proportions.

[4] In addition to the CO₂ cycle, Mars' atmosphere experiences other variations associated with the planetary rotation and the associated daily cycle. Mars' strong daily cycle is due to the low thermal inertia of the atmosphere and the strong solar heating during the day [Read and Lewis, 2004], with day-night temperature differences reaching 100K. The surface also has a low thermal capacity due to the absence of oceans, cooling rapidly as night falls, as in desert landscapes on Earth.

[5] Chao and Rubincam [1990] studied seasonal variations in Mars' gravitational field and rotation due to CO₂ exchange. They estimated peak-to-peak changes in J₂ and J₃ of $\sim 6 (10)^{-9}$ over a Martian year. A 30-mm peak-to-peak center of mass shift was estimated along the z axis. These changes were due to variations in the ice caps, the atmospheric effects for ΔJ_2 were estimated to be about 20% as large and in opposite phase. The investigation did not use outputs from a Mars atmospheric model, it assumed an instantaneous redistribution of CO₂ mass as well as axial symmetry of the polar caps.

[6] Smith *et al.* [1999] investigated the time variation of the long wavelength gravitational field of Mars due to mass redistribution associated with the annual cycle of CO₂

¹Planetary Geodynamics Laboratory, NASA Goddard Space Flight Center, Greenbelt, Maryland, USA.

²Space Geodesy Laboratory, NASA Goddard Space Flight Center, Greenbelt, Maryland, USA.

³Space Sciences Division, NASA Ames Research Center, Moffett Field, California, USA.

exchange between the atmosphere and polar caps. To that purpose they used monthly estimates of atmospheric pressure and polar frost as calculated by the NASA/Ames general circulation model. They predict changes in the planetary flattening and pear-shaped terms of the field, which could be detected from an orbital spacecraft. They used a version of the Ames GCM consisting of 13 vertical layers, extending from the surface up to a height of 45 km. The geopotential topography model used consisted of an 8th degree and order spherical harmonic model derived from Mariner 9 and Viking data, due to *Smith and Zuber* [1996]. The temporal analysis was based on twenty 33-day monthly averages of atmospheric pressure and CO₂ polar frost provided by the Ames GCM.

[7] *Yoder et al.* [2003] investigated the seasonal changes in zonal gravity coefficients, which arise from the variations in ice-cap growth and decay. They analyzed MGS radio tracking data to estimate variations in the second and third degree zonals.

[8] *Karatekin et al.* [2005] calculated and compared seasonal variations for the zonal coefficients of degree 2 to 5 based on the NASA/Ames GCM, the Laboratoire de Meteorologie Dynamique (LMD) GCM and the measurements of CO₂ deposit thickness by the High Energy Neutron Detector (HEND) on board the Mars Odyssey spacecraft. Although similar in general behavior, differences of 30% in the amplitude of the coefficients were found between the NASA Ames GCM, the LMD GCM and the HEND coefficients.

[9] They compared the estimated C₂₀ and C₃₀ coefficients from annual and semiannual solutions by *Smith et al.* [2001] and *Yoder et al.* [2003] based on perturbations of the MGS orbiter. Their results show differences in the tracking data solutions of up to 40% for C₂₀. They conclude that tracking data solutions do not discriminate between the models.

[10] They performed MGS tracking data simulations, which indicate that neglect of C₄₀ and C₅₀ maps into 50% effects on the solution for C₂₀ and C₃₀. These results lead them to conclude that the higher-degree terms should not be neglected in the determination procedure of seasonal gravity field variations from spacecraft tracking data.

[11] The main objective of this investigation is to make use of outputs from the NASA/Ames General Circulation Model (GCM) to compute and analyze the variations in Mars' gravitational field due to changes in the ice caps and the associated changes in the atmospheric mass distribution. The output from the NASA/Ames GCM incorporates other atmospheric effects as well, such as dust storms and the daily cycle. Those effects cause changes in the atmospheric mass distribution and the associated gravity field. Their determination and analysis is part of this investigation as well.

[12] This investigation makes use of the outputs from a recent version of the NASA/Ames GCM, with an extended vertical structure (30 layers extending from the surface up to a height of 100 km). *Sanchez et al.* [2003, 2004] used the outputs of this model to investigate the atmospheric rotational effects on Mars. This version was used by *Karatekin et al.* [2005] as well.

[13] The surface topography model is based on the precise topographic observations provided by the Mars Observer Laser Altimeter (MOLA) on the Mars Global Surveyor (MGS) spacecraft [*Smith et al.*, 2001]. Accuracy

in geopotential height is important since it plays a significant role in the processes leading to the formation and sublimation of CO₂ frost on the surface. This investigation makes use of the full spatial and temporal definition of the Ames GCM model. The 9° longitudinal definition allows up to a 40 degree and order spherical harmonic expansion ($n = 360^\circ/9^\circ$). The time series for the variation of the coefficients have a time step of 1.5 Martian hours, yielding 10704 points during a Martian year of 669 days. Therefore the Fourier analysis of the time series is not constrained to annual and semiannual harmonics only. The results of this investigation should help to inform future efforts based on spacecraft tracking data by providing information on the time history of the nominal values of the coefficients and their spectral structure.

[14] The structure of the paper is as follows. The basic equations are introduced in section 2. Section 3 is dedicated to the presentation of the results. Variations of the zonal coefficients are presented in section 3.1. Results for the sectorial and tesseral variations are discussed in section 3.2. First-degree variations and associated center of mass displacements are the topic of section 4. Comparisons to results by other investigations appear in section 5. The perturbations produced by the gravitational variations on the Mars Global Surveyor (MGS) orbiter are covered in section 6. Summary and conclusions appear in section 7.

2. Basic Equations

[15] The expressions for the variations of the spherical harmonic coefficients are well known, from *Lambeck* [1988],

$$(\Delta C_{nm}, \Delta S_{nm})^T = F_{nm} \int (r)^n P_{nm}(\sin \phi) (\cos m\lambda, \sin m\lambda)^T dm, \quad (1)$$

with

$$F_{nm} = (1 + k_n^1)(1/MR^n)(2 - \delta_{0m})[(n - m)!/(n + m)!], \quad (2)$$

where M is the mass of the planet, R denotes the mean planetary radius, (r, ϕ , λ) are the spherical coordinates of a mass element "dm", P_{nm} are the unnormalized Legendre polynomials, and T denotes the transpose operator. ΔC_{nm} and ΔS_{nm} symbolize variations of the Stokes coefficients of degree n and order m. The value of k_n¹ (the n-degree loading Love number) is weakly dependent on frequency. Mars is more rigid than Earth, and the loading Love numbers are relatively small and at the present time not that well determined owing to uncertainties in the knowledge of Mars' interior structure. In what follows, the computation of the variation of the coefficients is based on a rigid Mars (k_n¹ = 0), with the exception of the computation of MGS orbital perturbations where a value of k₂² = -0.06 [*Defraigne et al.*, 2000] has been adopted for the second-degree variations.

[16] The radial distance "r" to an element of mass can be approximated by

$$r = R - R \left[f(\sin \phi)^2 + (3/2)f^2(\sin \phi)^2 - (3/2)f^2(\sin \phi)^4 \right] + h, \quad (3)$$

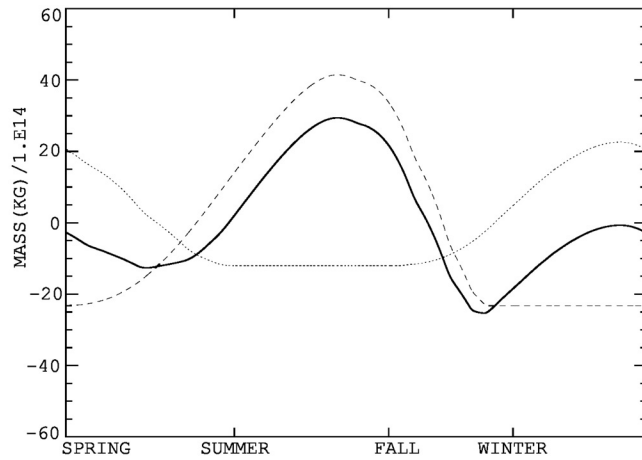


Figure 1. Ice mass variation time series. Seasons refer to Northern Hemisphere. Dotted line, northern ice cap; dashed line, southern ice cap; solid line, sum of both.

where, for Mars, the mean radius $R = 3,389,508$ m, and the polar flattening $f = 1/169.8$ [Smith *et al.*, 1999], “ h ” denotes the surface topography as specified in the atmospheric model. The volume integral in equation (1) is then reduced to a surface integral.

[17] The computation of the variation in the coefficients involves the evaluation of integrals containing the elements of mass. These are supplied by the NASA Ames GCM. They are given as separate contributions from surface ice condensation and atmospheric mass redistribution. The results are presented in terms of unnormalized coefficients since it is desired to compare the variations in the coefficients to each other.

[18] The paper presents the results of Fourier analysis of time series representing various quantities. For each pair of terms, $a_k \cos kt + b_k \sin kt = (a_k^2 + b_k^2)^{1/2} \cos(kt - \varphi)$, we refer to the quantity $(a_k^2 + b_k^2)^{1/2}$ as the “power at frequency k ”. A plot of this quantity as a function of k is called the power spectrum, as shown by Hamming [1986, p. 515]. Note that this convention makes the units of power the same as those of the particular time series under consideration; that is, if the time series refers to displacement in millimeters, then the units of power are millimeters also. When reference is made to “total power”, it means the sum over the entire frequency range.

[19] The variations of the coefficients are due to two effects, the changes in the polar caps and the variations in the mass distribution of the atmosphere. The two are given separately in the results that follow. Also given is the sum of the two, which is what would be detected by orbital perturbations or other measuring instruments.

[20] The variations in the coefficients (ΔC_{nm} , ΔS_{nm}) can be associated with displacements of the geoid [Caputo, 1967],

$$d_{Cnm} = R \Delta C_{nm} = R \sum [a_k \cos kt + b_k \sin kt]_{\Delta Cnm} \quad (4)$$

$$d_{Snm} = R \Delta S_{nm} = R \sum [a_k \cos kt + b_k \sin kt]_{\Delta Snm} \quad (5)$$

The results will be presented in this form also. The geoid displacements based on total power are then given by

$$d_{Cnm} = R \sum [(a_k^2 + b_k^2)^{1/2}]_{\Delta Cnm} \quad (6)$$

$$d_{Snm} = R \sum [(a_k^2 + b_k^2)^{1/2}]_{\Delta Snm}, \quad (7)$$

where the summation is taken over the total frequency range for each particular coefficient.

[21] The 9° longitudinal GCM grid definition allows up to a 40 degree and order spherical harmonic expansion. Such an expansion encompasses a total of 1680 coefficients (not including C_{00}). The present limits on the capabilities to measure the variations, the state of the art in the development of Mars GCMs and the small size of the variations allows the choice of a much smaller set for the presentation of most of the results.

[22] Many of the results are presented in terms of the Northern Hemisphere seasons. In terms of Martian days, the initial points are spring (0 sols), summer (194 sols), fall (372 sols) and winter (515 sols).

3. Results

3.1. Zonal Variations

[23] Examination of equation (1) indicates that time dependency occurs only through the time series for the elements of mass “ dm .” The outputs of the NASA/Ames GCM allow the computation of the mass variation associated with the ice caps and with the atmospheric mass. A Northern/Southern Hemisphere analysis brings into relief the seasonal effects. Such effects should be associated with variations in the zonal coefficients. The resulting time series are shown in Figures 1 and 2. The results of harmonic analysis of the associated time series are given in Table 1. Several conclusions can be drawn from the results.

[24] 1. The magnitude of the mass variation in the southern ice cap is approximately twice the magnitude in the northern ice cap.

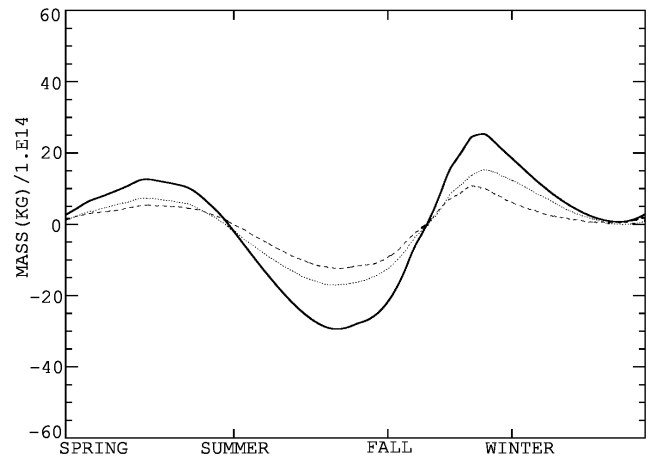


Figure 2. Atmospheric mass variation time series. Dotted line, Northern Hemisphere; dashed line, Southern Hemisphere; solid line, sum of both.

Table 1. Harmonic Analysis Results of Time Series for Mass Variations in the Ice Caps and the Atmosphere^a

Mass Variation	Main Harmonics, Cycles Per Year (Amplitude, 10 ¹⁴ Kg) (Phase Angle, degrees)		
	South	North	Both
Ice Caps	1 (16.34) (-168°)	1 (8.65) (5°)	1 (7.70) (-160°)
	2 (5.01) (38°)	2 (2.68) (13°)	2 (7.65) (31°)
	3 (1.71) (119°)	3 (0.13) (-93°)	3 (1.66) (134°)
	4 (0.71) (162°)	4 (0.10) (-96°)	4 (0.81) (-109°)
	5 (0.42) (58°)	5 (0.12) (-88°)	5 (0.46) (39°)
	6 (0.21) (99°)	6 (0.04) (-87°)	6 (0.24) (104°)
	7 (0.06) (99°)	7 (0.02) (-95°)	7 (0.09) (138°)
	8 (0.10) (89°)	8 (0.04) (-98°)	8 (0.07) (130°)
	9 (0.11) (77°)	9 (0.05) (-92°)	9 (0.15) (68°)
	10 (0.09) (107°)	10 (0.04) (-85°)	10 (0.10) (122°)
Air Mass	1 (3.05) (18°)	1 (4.66) (21°)	1 (7.70) (20°)
	2 (3.17) (-148°)	2 (4.48) (-150°)	2 (7.65) (-149°)
	3 (0.86) (-25°)	3 (0.88) (-64°)	3 (1.66) (-46°)
	4 (0.45) (82°)	4 (0.37) (52°)	4 (0.81) (71°)
	5 (0.26) (-147°)	5 (0.20) (-137°)	5 (0.46) (-142°)
	6 (0.13) (-55°)	6 (0.12) (-90°)	6 (0.24) (-76°)
	7 (0.06) (22°)	7 (0.04) (-65°)	7 (0.09) (-42°)
	8 (0.03) (84°)	8 (0.04) (-58°)	8 (0.07) (-49°)
	9 (0.07) (-115°)	9 (0.08) (-112°)	9 (0.15) (-113°)
	10 (0.04) (-40°)	10 (0.05) (-68°)	10 (0.10) (-58°)

^aResults for the Northern and Southern Hemispheres and for the sum of both hemispheres.

[25] 2. The annual harmonics for the northern and southern ice caps are 173° out of phase, they subtract to produce the total annual resultant, which is only 0.13% greater than a 100% out-of-phase resultant. The semiannual harmonics are 25° out of phase; they add to produce the total semiannual resultant, which is only 0.52% less than a 100% in-phase resultant. The resultant of the (1/3)-annual harmonics is

only 5% greater than a 100% out-of-phase resultant. The resultant of the (1/4)-annual harmonics is equal to a 100% in-phase resultant.

[26] 3. The magnitude of the atmospheric mass variation in the Northern Hemisphere is approximately 31% larger than the magnitude in the Southern Hemisphere.

[27] 4. The first 10 harmonics for atmospheric mass variation in the Northern and Southern Hemispheres are in phase, they add to produce the harmonics for the total.

[28] 5. The total mass variations for the atmosphere and ice caps satisfy conservation of mass.

[29] To gain further understanding about the variation in the ice caps it is useful to compute and display the spatial and temporal variation in ice thickness. Figure 3 exhibits the variation in ice thickness as a function of latitude for each of the Northern Hemisphere seasons. Every latitude point corresponds to the average seasonal value for the corresponding latitude band. Positive/negative latitude points correspond to the northern/southern ice cap. As expected the maximum/minimum ice thickness occurs in the corresponding winter/summer season for the particular hemisphere. Spring and fall averages show the presence of ice in both hemispheres. At this point it is pertinent to recall that the computations do not include any permanent ice cover. Some of the numbers associated with the computations are as follows: The northern spring season ice thickness has a maximum of 27.5 cm, which occurs at 82.5° north latitude. The northern summer maximum of 48.8 cm occurs at -90° (South Pole winter). The northern fall maximum of 37 cm occurs at the South Pole as well. The northern winter maximum of 31.3 cm covers the range 82.5°-90° in the Northern Hemisphere. The ice thickness

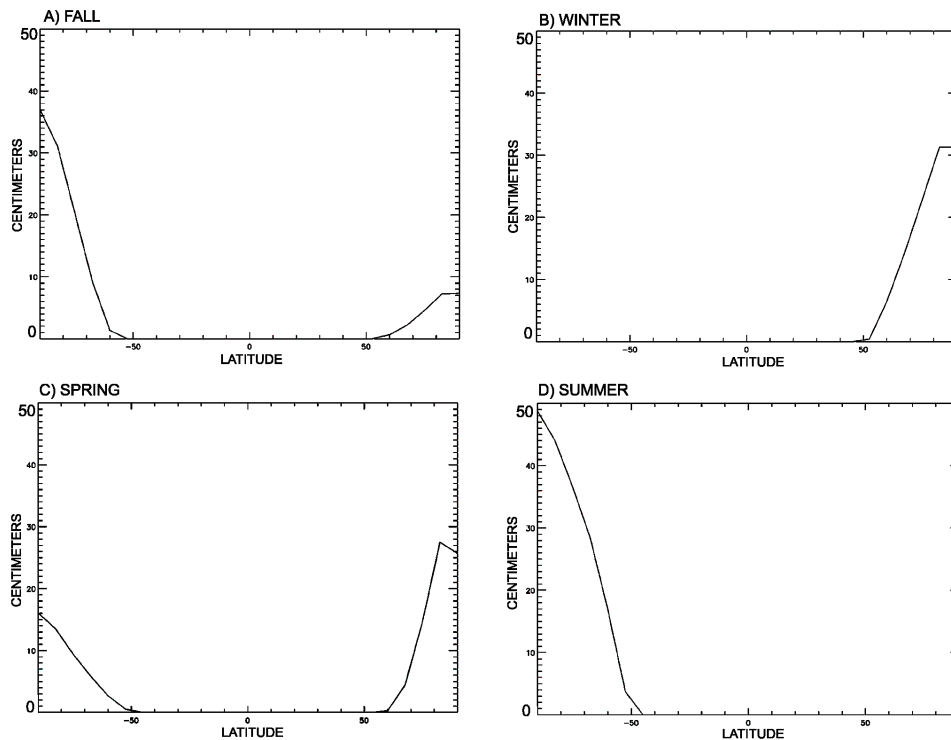


Figure 3. Variation in ice thickness as a function of latitude. Average seasonal values for the corresponding latitude band. (a) Fall. (b) Winter. (c) Spring. (d) Summer.

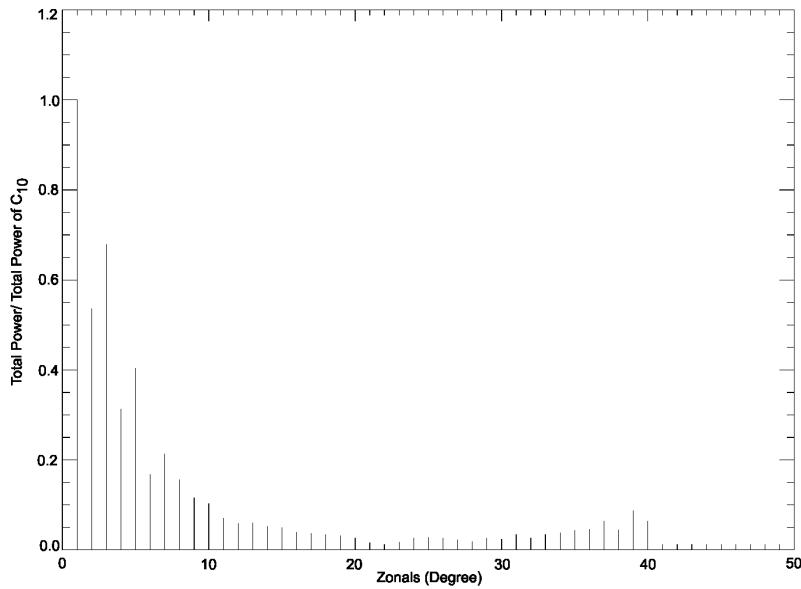


Figure 4. Total power ranking of the variation in 40 zonal coefficients as a fraction of ΔC_{10} .

variations as a function of latitude are associated with variations in the zonal coefficients of the gravitational potential.

[30] Figure 4 shows the power ranking of the 40 zonal variations as a fraction of ΔC_{10} . The least powerful is the 22nd degree zonal, with an equivalent geoid displacement of 0.37 mm, the largest is ΔC_{10} (34.9 mm). Figures 5 and 6 exhibit the time series for the eight most powerful zonal variations. These figures show the contributions due to the

northern and southern ice caps, as well as the atmospheric mass contribution and the combined total.

[31] Table 2 lists the total power for the 16 most powerful zonal variations. The power has been expressed in terms of millimeters of geoid displacement (equation (6)). Results are given for the atmospheric and ice caps effects separately and in combination. The most powerful variation is that of ΔC_{10} , followed by ΔC_{30} and ΔC_{20} . The ice caps' total power is larger than the atmospheric total power in every

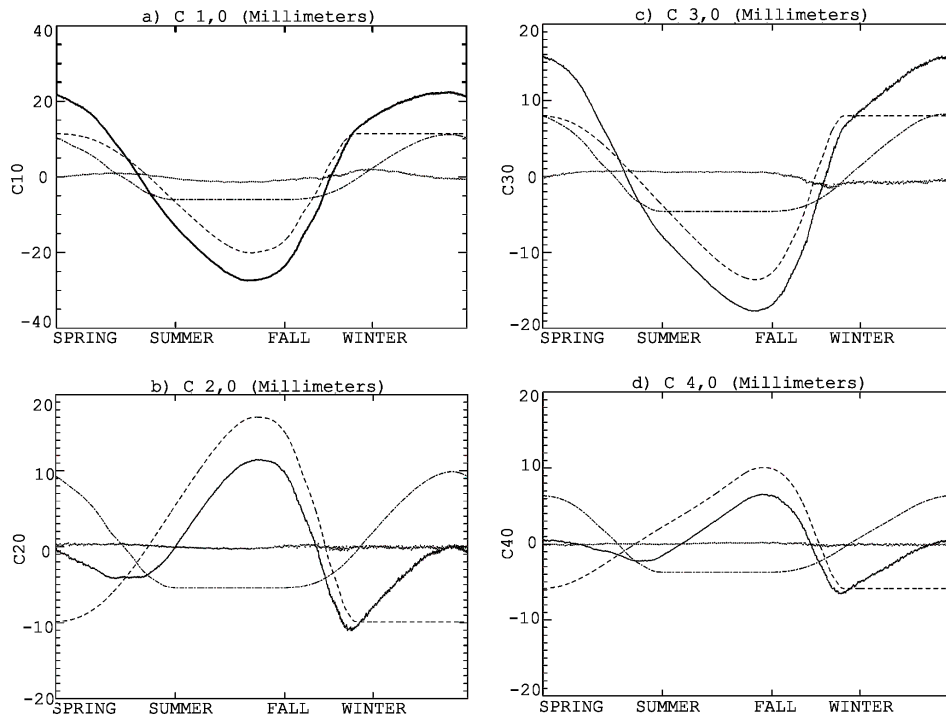


Figure 5. Time series for variation in zonal coefficients. Units are millimeters of geoid displacement. (a) ΔC_{10} . (b) ΔC_{20} . (c) ΔC_{30} . (d) ΔC_{40} . Dotted line, atmosphere; dashed line, southern ice cap; dash-dotted line, northern ice cap; solid line, sum of atmosphere and ice caps.

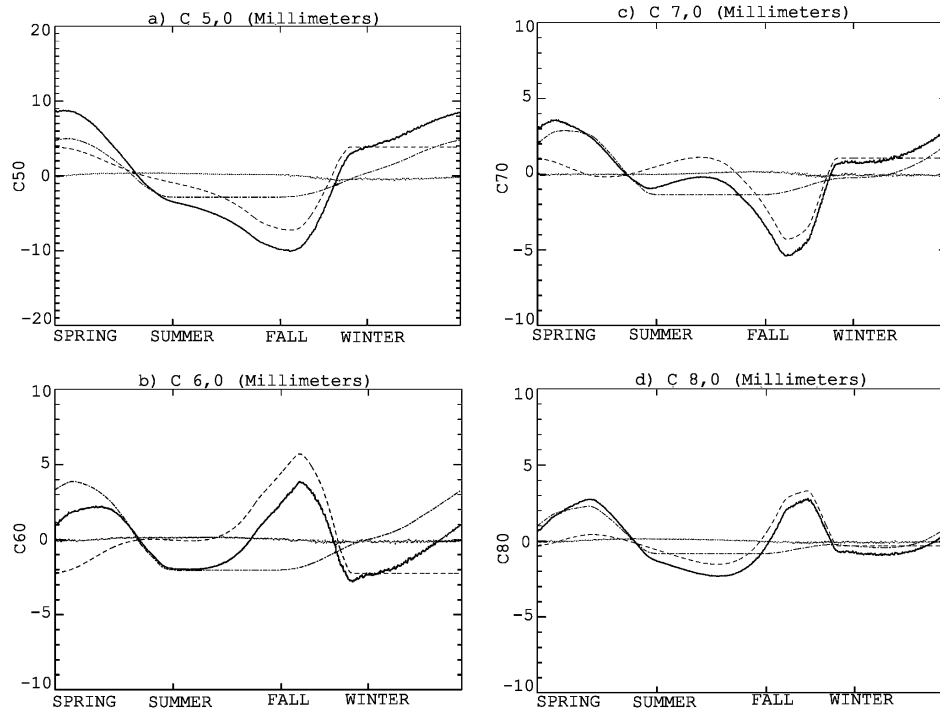


Figure 6. Time series for variation in zonal coefficients. (a) ΔC_{50} . (b) ΔC_{60} . (c) ΔC_{70} . (d) ΔC_{80} . Line types are as in Figure 5.

case. Note also that their sum is larger than 100%, indicating that some power is lost to competing effects, which are out of phase.

[32] Table 3 lists the amplitude and frequency of the three main harmonics for atmospheric and ice caps effects in combination. Note that the main harmonic for the odd degree zonal variations is the annual. This was noted and explained by *Smith et al.* [1999] for ΔC_{10} and ΔC_{30} as the result of constructive (in phase) ice deposition in the winter pole and sublimation at the summer pole. However, Table 3 shows that for the 11th and 13th degree zonal variations the main harmonic is the (1/3)-annual. For the 37th and 39th

Table 3. Amplitude and Frequency of the Three Main Harmonics for the Atmospheric and Ice Effects in Combination for the 16 Largest Zonal Variations

Zonal Variation Degree	Atmosphere + Ice Main Harmonics, Cycles per Year (Amplitude, mm)		
	First Harmonic	Second Harmonic	Third Harmonic
1	1 (12.7)	2 (1.58)	3 (0.99)
2	2 (3.08)	1 (2.94)	3 (0.78)
3	1 (8.36)	3 (0.96)	2 (0.63)
4	2 (1.83)	1 (1.30)	3 (0.57)
5	1 (4.24)	3 (0.90)	2 (0.46)
6	2 (1.21)	4 (0.31)	3 (0.29)
7	1 (1.40)	3 (0.65)	2 (0.41)
8	2 (0.95)	1 (0.46)	4 (0.31)
9	1 (0.51)	3 (0.39)	2 (0.20)
10	2 (0.48)	1 (0.28)	4 (0.24)
11	3 (0.28)	1 (0.16)	2 (0.13)
12	2 (0.14)	4 (0.14)	1 (0.12)
13	3 (0.18)	1 (0.15)	2 (0.11)
37	1 (0.41)	3 (0.20)	2 (0.10)
39	1 (0.82)	3 (0.21)	2 (0.11)
40	2 (0.34)	1 (0.26)	3 (0.12)

Table 2. Total Power for the 16 Largest Zonal Variations^a

Zonal Variation Degree (% of C_{10})	Total Power, Millimeters of Geoid Displacement (Percent of Atmosphere + Ice)		
	Atmosphere	Ice	Atmosphere + Ice
1 (100%)	5.16 (14.7%)	31.20 (89.3%)	34.92
2 (53.5%)	3.38 (18.0%)	16.23 (86.7%)	18.71
3 (67.9%)	3.97 (16.7%)	22.68 (95.6%)	23.71
4 (31.3%)	2.00 (18.3%)	9.17 (83.8%)	10.94
5 (40.3%)	2.06 (14.6%)	13.28 (94.3%)	14.08
6 (16.8%)	1.40 (23.8%)	4.91 (83.7%)	5.87
7 (21.2%)	1.20 (16.2%)	6.64 (89.3%)	7.43
8 (15.5%)	0.96 (17.8%)	4.85 (89.4%)	5.43
9 (11.5%)	0.67 (16.6%)	3.52 (87.0%)	4.04
10 (10.2%)	0.57 (16.0%)	3.22 (90.0%)	3.58
11 (7.0%)	0.49 (19.9%)	2.11 (85.5%)	2.47
12 (5.8%)	0.43 (21.0%)	1.75 (85.5%)	2.05
13 (6.0%)	0.36 (17.3%)	1.87 (89.0%)	2.10
37 (6.3%)	0.32 (14.6%)	2.05 (92.6%)	2.21
39 (8.6%)	0.39 (13.0%)	2.88 (95.1%)	3.02
40 (6.4%)	0.37 (16.6%)	2.03 (90.3%)	2.25

^aDisplacement of the geoid due to the contributions of the atmosphere, the ice caps, and the sum of both.

Table 4. Frequency, Amplitude, and Phase of the Main Zonal Harmonics for Variation in Each of the Ice Caps and for the Sum of Both^a

Zonal Variation Degree of Expansion	Main Harmonics, Cycles Per Year (Amplitude, mm) (Phase Angle, degrees)		
	South Cap	North Cap	Both Caps
1	1 (7.97) (12°)	1 (4.30) (5°)	1 (12.2) (9°)
	2 (2.40) (-145°)	2 (1.31) (11°)	2 (1.17) (-130°)
	3 (0.89) (-62°)	3 (0.09) (-92°)	3 (0.95) (-69°)
	4 (0.36) (-2°)	4 (0.05) (-96°)	4 (0.32) (-80°)
2	1 (6.82) (-169°)	1 (3.84) (5°)	1 (2.99) (-162°)
	2 (2.00) (30°)	2 (1.12) (8°)	2 (3.11) (23°)
	3 (0.87) (116°)	3 (0.13) (-89°)	3 (0.77) (128°)
	4 (0.35) (-165°)	4 (0.04) (-96°)	4 (0.39) (-117°)
3	1 (5.36) (9°)	1 (3.24) (5°)	1 (8.59) (8°)
	2 (1.54) (-161°)	2 (0.90) (2°)	2 (0.74) (-144°)
	3 (0.83) (-67°)	3 (0.17) (-87°)	3 (0.99) (-72°)
	4 (0.33) (24°)	4 (0.03) (-98°)	4 (0.29) (-42°)
4	1 (3.81) (-173°)	1 (2.57) (5°)	1 (1.24) (-171°)
	2 (1.14) (0°)	2 (0.69) (-6°)	2 (1.80) (-2°)
	3 (0.76) (108°)	3 (0.22) (-85°)	3 (0.55) (114°)
	4 (0.30) (-154°)	4 (0.03) (-104°)	4 (0.33) (-138°)
5	1 (2.40) (2°)	1 (1.92) (6°)	1 (4.32) (4°)
	2 (0.91) (148°)	2 (0.53) (-17°)	2 (0.51) (121°)
	3 (0.67) (-79°)	3 (0.24) (-85°)	3 (0.91) (-81°)
	4 (0.29) (23°)	4 (0.03) (-133°)	4 (0.26) (18°)
6	1 (1.28) (174°)	1 (1.34) (6°)	1 (0.07) (77°)
	2 (0.80) (-65°)	2 (0.44) (-31°)	2 (1.21) (-53°)
	3 (0.55) (90°)	3 (0.25) (-88°)	3 (0.29) (89°)
	4 (0.28) (-163°)	4 (0.03) (145°)	4 (0.31) (-169°)
7	1 (0.56) (-26°)	1 (0.88) (7°)	1 (1.43) (-6°)
	2 (0.72) (93°)	2 (0.40) (-49°)	2 (0.40) (72°)
	3 (0.42) (-107°)	3 (0.23) (-97°)	3 (0.65) (-104°)
	4 (0.27) (9°)	4 (0.04) (126°)	4 (0.23) (25°)
8	1 (0.32) (99°)	1 (0.55) (7°)	1 (0.48) (34°)
	2 (0.60) (-102°)	2 (0.37) (-70°)	2 (0.95) (-93°)
	3 (0.31) (48°)	3 (0.20) (-116°)	3 (0.16) (39°)
	4 (0.25) (179°)	4 (0.05) (124°)	4 (0.31) (165°)

^aPhase rounded to the nearest degree.

degree zonal variations the main harmonic is again the annual. The power gap between the main annual harmonic and the second-rank harmonic is large for the 1st and 3rd degree zonals. It is not as large for the higher degree odd-zonals. The second-rank harmonic for the odd-zonal variations is generally the (1/3)-annual, with the exception of ΔC_{10} (semiannual) and the 11th and 13th degree zonals (annual). Table 3 shows the (1/2)-annual as the main harmonic for all the even zonal variations. This was noted and explained by *Smith et al.* [1999] for ΔC_{20} as a result of competing (out of phase) ice deposition/sublimation effects in the winter/summer pole. Note however, that the power gap between the first (1/2)-annual harmonic and the second-rank annual harmonic is not very large (in the case of ΔC_{20} they are almost equal). The second-rank harmonic for the even-zonal variations is generally the annual, except for ΔC_{60} and the 12th degree zonal, which show a (1/4)-annual harmonic in second rank.

[33] The results shown in Tables 2 and 3 indicate that the ice caps effect is the most important in the combined (atmospheric plus ice) variations. Some of the largest displacements as given by equation (4) (and shown in Figures 5 and 6) are -27.5 mm (ΔC_{10}), -17.7 mm (ΔC_{30}), 11.4 mm (ΔC_{20}) and -10.0 mm (ΔC_{50}).

[34] Examination of the Fourier analysis results yields a general rule for correlation between the separate contribu-

tions of the northern and southern ice caps. That is, a rule connecting the amplitudes and phases of the different time harmonics appearing in the spectrum of the various zonal variations.

[35] The separate contributions due to the northern and southern ice caps combine differently for the even and odd zonal variations. *Smith et al.* [1999] noted this from their graphs for the first, second and third-degree zonal variations and it is evident also in Figures 5 and 6. The tools used in this investigation allow a more extended and quantitative analysis. The results are presented in Table 4, which lists the amplitude, phase and frequency of the main harmonics for each of the caps and for the sum of the two, for the zonal variations. Examination of the data for the eight most powerful zonal variations allows the following conclusions with respect to the contributions of the northern and southern ice caps: (1) The first two even time harmonics (2 and 4 cycles per year) are in/out of phase for the even/odd degree zonal variations. (2) The first two odd time harmonics (1 and 3 cycles per year) are in/out of phase for the odd/even degree zonal variations. To understand these results it is helpful to recall some of the developments with respect to mass variation in the ice caps.

[36] 1. The first two odd time harmonics (1 and 3 cycles per year) are out of phase for the mass variations in the northern and southern ice caps. The first two even time harmonics (2 and 4 cycles per year) are in phase for the mass variations in the northern and southern ice caps.

[37] 2. The behavior of the Legendre polynomials P_n (sin ϕ) as a function of latitude and degree “n” in combination with the rules for mass variation in the northern and southern ice caps yield the rules for the zonal gravitational variations due to the northern and southern ice caps.

3.2. Sectorial and Tesseral Variations

[38] Another way to analyze the ice thickness variations is to compute averages on longitudinal segments. Longitudinal time variations in ice thickness with respect to the longitudinal annual average will occur as a function of the atmospheric dynamics. There are mass variations associated with the ice thickness variations. Figure 7 exhibits the seasonal longitudinal ice mass variation averages for the northern and southern hemispheres. Figure 7 also shows the longitudinal averages for the Mars topography used by the NASA/Ames atmospheric model. Examination of Figure 7a for the Northern Hemisphere does not indicate a strong correlation between variations in topography and ice mass variation. There seems to be a negative correlation between ice mass variation during summer-fall and spring-winter. The same negative seasonal correlation is evident in the southern hemisphere (Figure 7b).

[39] It is evident that there are seasonal differences as well as geographic (north/south and longitudinal) differences. The ice mass variations as a function of longitude should result in time variations in the tesseral and sectorial coefficients of the gravitational potential.

[40] Similarly, a longitudinal analysis of the air mass variations can be performed. Longitudinal time variations in air mass with respect to the longitudinal annual average will occur as a function of the atmospheric dynamics. Figure 8 exhibits the seasonal longitudinal atmospheric mass variation averages for the northern and southern

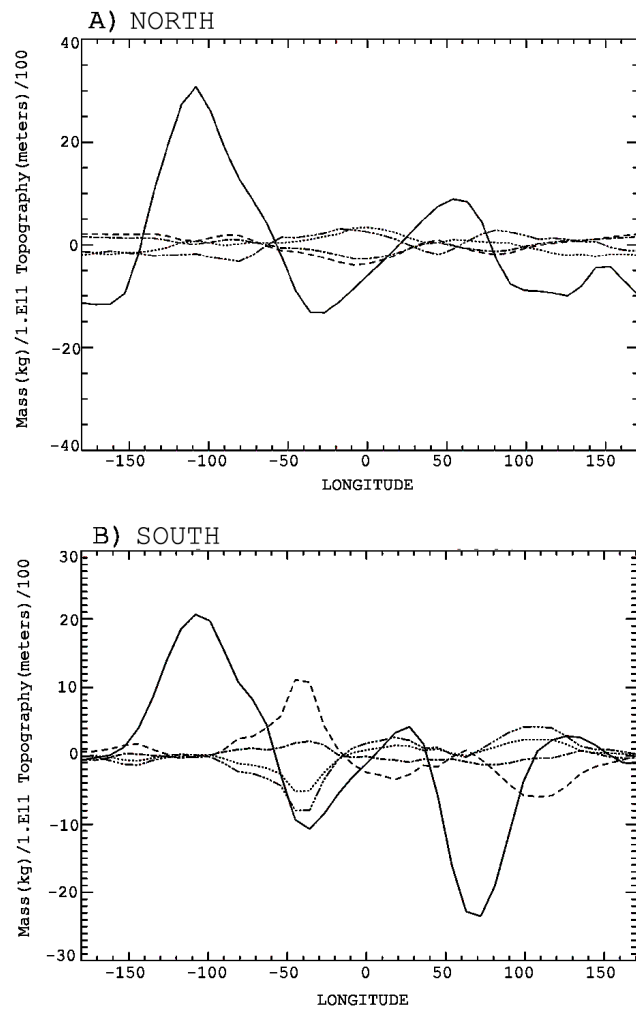


Figure 7. Seasonal longitudinal ice mass variation averages in $\text{kg}/(10^{11})$. (a) Northern Hemisphere. (b) Southern Hemisphere. Solid line, topography in meters/100; dotted line, spring; dashed line, summer; dash-dotted line, fall; dash-dot-dot-dotted line, winter.

hemispheres, as well as the topographic variations. Examination of Figure 8a for the northern hemisphere indicates a strong positive correlation between variations in topography and air mass variations during the summer. The correlation is negative between topographic variation and air mass variation during fall, winter and spring, albeit less strong than during summer.

[41] Examination of Figure 8b for the Southern Hemisphere indicates a negative correlation between topographic variation and air mass variation during the spring. There is positive correlation between topographic variation and air mass variation during summer, fall and winter. However, the correlation between summer air mass and topographic variations become negative in the segment between 50° and 90° longitude.

[42] The figure shows clearly that there are seasonal differences as well as geographic differences. The longitudinal air mass variations will result in time variations of the tesseral and sectorial coefficients of the gravitational potential.

[43] Comparison of Figures 1 and 7 shows that the zonal ice mass seasonal variations are about 4 orders of magnitude larger than the longitudinal ice mass seasonal variations. Comparison of Figures 2 and 8 shows that the zonal air mass seasonal variations are about 4 orders of magnitude larger than the longitudinal air mass seasonal variations. It is to be expected that the zonal coefficients' seasonal variations will be much larger than the sectorial and tesseral seasonal variations.

[44] To focus on the rotational effects, a division into western/eastern hemispheres is more appropriate. The results from harmonic analysis are presented in Table 5 and summarized below.

[45] 1. The magnitude of the corresponding mass variation harmonics in the east and west hemispheres is approximately equal, especially for the atmospheric variations.

[46] 2. The first four time harmonics are in phase for the mass variations in the east and west hemispheres. This is true for the ice caps and the atmospheric mass variations.

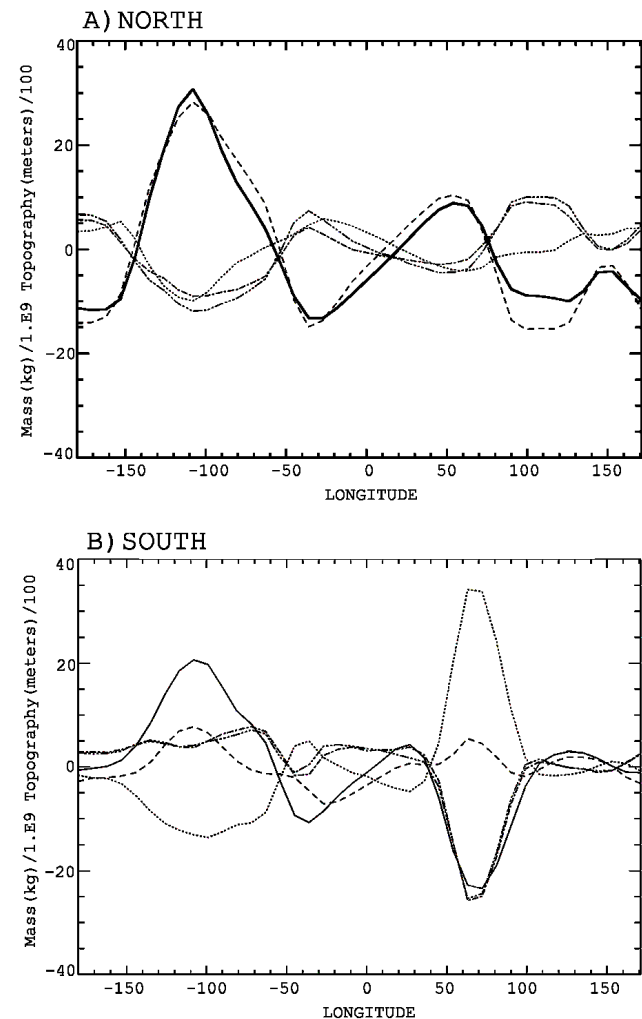


Figure 8. Seasonal longitudinal air mass variation averages in $\text{kg}/(10^9)$. (a) Northern Hemisphere. (b) Southern Hemisphere. Solid line, topography in meters/100; dotted line, spring; dashed line, summer; dash-dotted line, fall; dash-dot-dot-dotted line, winter.

Table 5. Harmonic Analysis Results of Time Series for Mass Variations in the Ice Caps and the Atmosphere^a

Mass Variation	Main Harmonics, Cycles Per Year (Amplitude, 10 ¹⁴ Kg) (Phase Angle, degrees)		
	East	West	Both
Ice Caps	1 (3.40) (-158°)	1 (4.30) (-161°)	1 (7.70) (-160°)
	2 (3.66) (32°)	2 (3.99) (30°)	2 (7.65) (31°)
	3 (0.78) (136°)	3 (0.88) (132°)	3 (1.66) (134°)
	4 (0.39) (-106°)	4 (0.42) (-112°)	4 (0.81) (-109°)
	669 (0.009) (0°)	669 (0.009) (176°)	669 (0.0004) (120°)
Air Mass	1 (3.81) (19°)	1 (3.90) (21°)	1 (7.70) (20°)
	2 (3.87) (-150°)	2 (3.78) (-148°)	2 (7.65) (-149°)
	3 (0.83) (-44°)	3 (0.82) (-48°)	3 (1.66) (-46°)
	4 (0.38) (71°)	4 (0.43) (71°)	4 (0.81) (71°)
	669 (0.10) (94°)	669 (0.10) (-86°)	669 (0.0002) (-69°)

^aResults for the eastern and western hemispheres and for the sum of both hemispheres.

[47] 3. The daily harmonics are out of phase for the atmospheric and ice mass variations in the east and west hemispheres.

[48] 4. The magnitude of the annual and semiannual ice mass harmonics is more than two orders of magnitude larger than the magnitude of the daily harmonics for the variations in the east and west hemispheres.

[49] 5. The magnitude of the annual and semiannual air mass harmonics is more than an order of magnitude larger than the magnitude of the daily harmonics for the variations in the east and west hemispheres.

Note the amplitude of the daily harmonics, which is comparable to those of the longitudinal seasonal variations.

[50] Figure 9 shows the power ranking of the most powerful sectorial and tesseral variations as a fraction of ΔC_{11} . Figures 10 and 11 display the time series for some of the most powerful sectorial and tesseral variations. These figures show the total contribution due to ice caps, as well as the combined total, including the atmospheric effects.

[51] Table 6 lists the total power associated with each of them. The largest variations are associated with the first-

degree coefficients ΔC_{11} and ΔS_{11} . Note that the atmospheric variations are more powerful than the ice caps variations, especially for the second-order coefficients ΔC_{22} , ΔS_{22} , ΔC_{32} , and ΔS_{32} .

[52] Table 7 lists the three main harmonics for the combined effect (atmosphere plus ice) and the amplitude of geoid displacement associated with each. The annual harmonic is the most powerful for all the variations, with the exception of ΔC_{11} (daily). Power is more diffused than for the zonal variations, with smaller percentages associated with the main harmonics. Note also the appearance of daily and (1/2)-daily harmonics in the top three.

[53] Examination of Figures 10 and 11 shows a change in the sectorial and tesseral variations as a function of the seasons. There is a difference in the spectrum of the spring-summer time span as compared to the fall-winter interval. The latter corresponds to the time of occurrence of global dust storms.

4. First Degree Variations

[54] The ΔC_{11} , ΔS_{11} and ΔC_{10} variations are associated with displacements of the center of mass (Δx_{cm} , Δy_{cm} , Δz_{cm}) from the origin of the coordinate system. The displacements are given by

$$\Delta x_{cm} = R \Delta C_{11}, \quad (8)$$

$$\Delta y_{cm} = R \Delta S_{11}, \quad (9)$$

$$\Delta z_{cm} = R \Delta C_{10}. \quad (10)$$

[55] The ΔC_{10} variation is the largest of all. In terms of total power, $\Delta C_{10} = 1.03016(10^{-8})$, which is equivalent to 34.9 mm of center of mass displacement (equation (6), Table 2). Table 2 gives similar information for ΔC_{10} due to

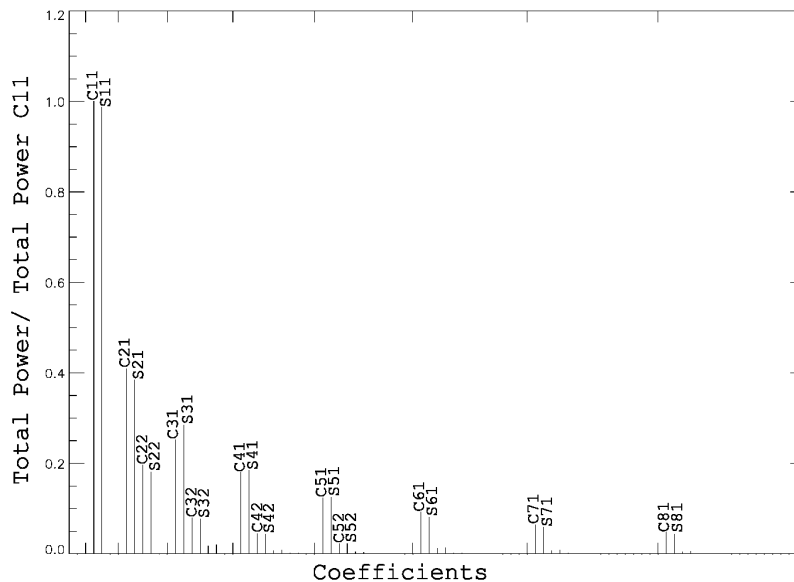


Figure 9. Total power ranking of the variation in sectorial and tesseral coefficients as a fraction of ΔC_{11} .

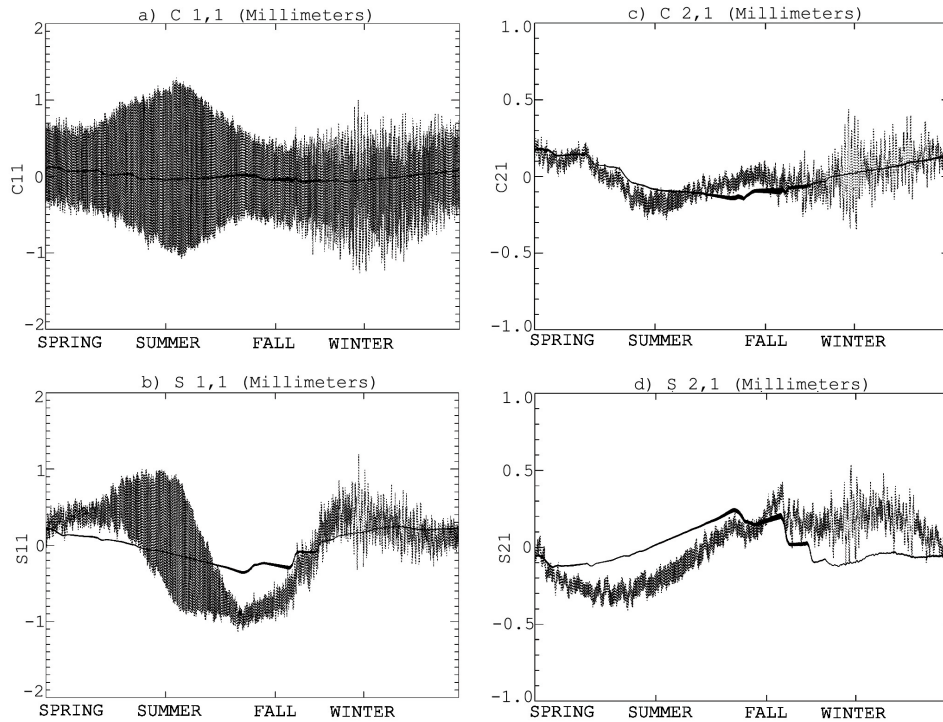


Figure 10. Time series for variation in sectorial and tesseral coefficients. Units are millimeters of geoid displacement. (a) ΔC_{11} . (b) ΔS_{11} . (c) ΔC_{21} . (d) ΔS_{21} . Solid line, ice mass contribution; dashed line, atmospheric plus ice.

the atmospheric and ice caps contributions separately. In terms of center of mass displacement, the atmospheric total power is equivalent to 5.16 mm, for the ice caps the displacement is 31.2 mm. From Table 2 we see that the

atmosphere’s total power is 14.7% of the sum of the two while the ice caps’ total power is 89.3% of the sum. The numbers indicate that 4% is “lost” to interference or cancellation between the two effects.

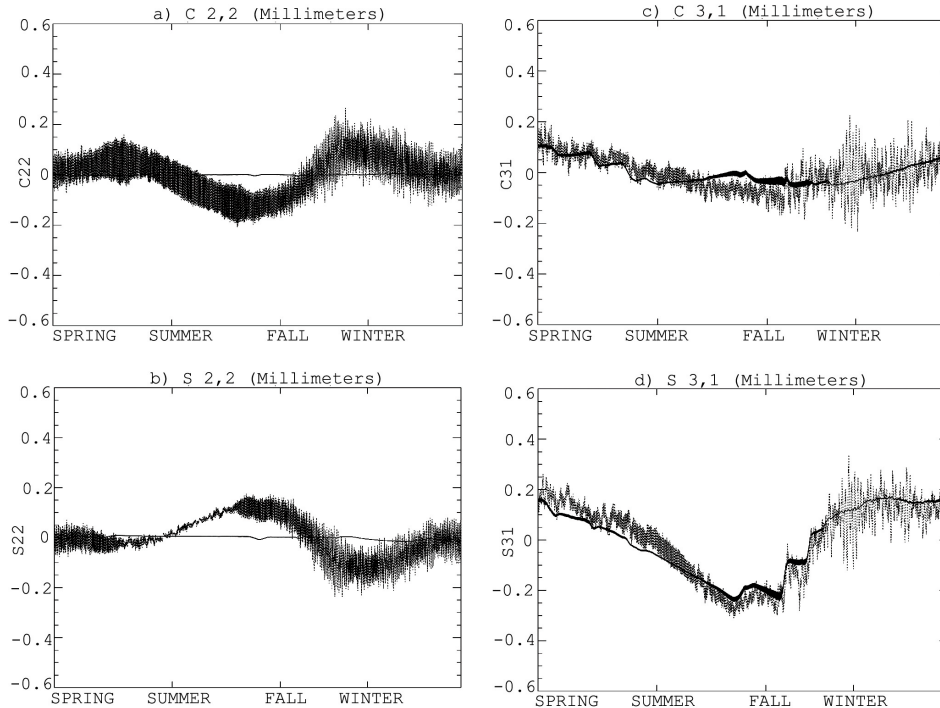


Figure 11. Time series for variation in sectorial and tesseral coefficients. (a) ΔC_{22} . (b) ΔS_{22} . (c) ΔC_{31} . (d) ΔS_{31} . Line types are as in Figure 10.

Table 6. Total Power for the Largest Sectorial and Tesseral Variations^a

Variation (Percent of C ₁₀)	Total Power, Millimeters of Geoid Displacement (Percent of Atmosphere + Ice)		
	Atmosphere	Ice	Atmosphere + Ice
C ₁₁ (13.4%)	4.59 (98.0%)	0.28 (6.0%)	4.68
S ₁₁ (13.2%)	4.28 (92.4%)	0.57 (12.4%)	4.63
C ₂₁ (5.4%)	1.78 (93.0%)	0.33 (17.5%)	1.91
S ₂₁ (5.1%)	1.66 (92.2%)	0.45 (24.9%)	1.80
C ₂₂ (2.6%)	0.91 (99.6%)	0.01 (1.8%)	0.92
S ₂₂ (2.4%)	0.83 (98.8%)	0.03 (4.2%)	0.84
C ₃₁ (3.3%)	1.11 (93.8%)	0.22 (19.3%)	1.18
S ₃₁ (3.8%)	1.08 (81.5%)	0.41 (30.7%)	1.33
C ₃₂ (1.0%)	0.36 (99.1%)	0.01 (4.3%)	0.37
S ₃₂ (1.0%)	0.34 (96.2%)	0.03 (9.3%)	0.36
C ₄₁ (2.4%)	0.69 (81.7%)	0.24 (29.3%)	0.84
S ₄₁ (2.4%)	0.68 (79.4%)	0.27 (31.2%)	0.86
C ₅₁ (1.6%)	0.48 (84.6%)	0.17 (29.9%)	0.57
S ₅₁ (1.6%)	0.49 (83.5%)	0.22 (38.0%)	0.58
C ₆₁ (1.2%)	0.33 (76.8%)	0.16 (39.0%)	0.43
S ₆₁ (1.0%)	0.33 (86.8%)	0.13 (34.2%)	0.38

^aDisplacement of the geoid due to the contributions of the atmosphere, the ice caps and the sum of both.

[56] The minimum displacement (equation (10)) is -27.5 mm, Figure 5 shows that it occurs at 310 sols, which corresponds to the second part of the summer in the Northern Hemisphere (194–372 sols). The maximum

Table 7. Amplitude and Frequency of the Three Main Harmonics for the Atmospheric and Ice Effects in Combination for the Largest Sectorial and Tesseral Variations

Variation	Atmosphere + Ice Main Harmonics, Cycles per Year (Amplitude, mm)		
	First Harmonic	Second Harmonic	Third Harmonic
C 1 1	669 (0.31)	1 (0.08)	671 (0.06)
S 1 1	1 (0.25)	2 (0.19)	669 (0.09)
C 2 1	1 (0.05)	2 (0.03)	669 (0.02)
S 2 1	1 (0.12)	2 (0.03)	669 (0.02)
C 2 2	1 (0.03)	2 (0.03)	1338 (0.02)
S 2 2	1 (0.03)	2 (0.03)	1338 (0.01)
C 3 1	1 (0.03)	669 (0.01)	2 (0.006)
S 3 1	1 (0.09)	2 (0.03)	669 (0.01)
C 3 2	1 (0.008)	2 (0.007)	3 (0.001)
S 3 2	1 (0.01)	2 (0.007)	3 (0.002)
C 4 1	1 (0.05)	2 (0.01)	3 (0.01)
S 4 1	1 (0.03)	2 (0.01)	3 (0.01)
C 5 1	1 (0.02)	2 (0.01)	3 (0.003)
S 5 1	1 (0.04)	2 (0.01)	3 (0.006)
C 6 1	1 (0.03)	3 (0.008)	2 (0.007)
S 6 1	1 (0.01)	2 (0.007)	3 (0.007)

displacement is 22.3 mm at 641 sols during Northern Hemisphere winter (515–669 sols).

[57] Table 3 lists the three most powerful harmonics. The main harmonics are annual, (1/2)-annual and (1/3)-annual for both effects combined but the annual harmonic is dominant with 12.7 mm amplitude.

[58] The sectorial variations of first degree and order are the largest of all the sectorial and tesseral variations, as shown in Table 6. They are determined mainly by the atmospheric contributions, with amplitudes of 4.59 mm (C₁₁) and 4.28 mm (S₁₁) of total power. The equatorial displacements of the center of mass associated with equations (8) and (9) can be expressed in terms of an equatorial vector of magnitude V_{cm} and phase Φ_{cm} ,

$$V_{cm} = R(\Delta C_{11}^2 + \Delta S_{11}^2)^{1/2} \quad (11)$$

$$\Phi_{cm} = \arctan(\Delta S_{11}/\Delta C_{11}). \quad (12)$$

[59] The corresponding time series for the variations are shown in Figure 12. Spectral analysis of the displacement time series (V_{cm}) yields main annual and semiannual harmonics. The associated amplitudes are 0.253 mm (annual) and 0.195 mm (semiannual). Next in magnitude are

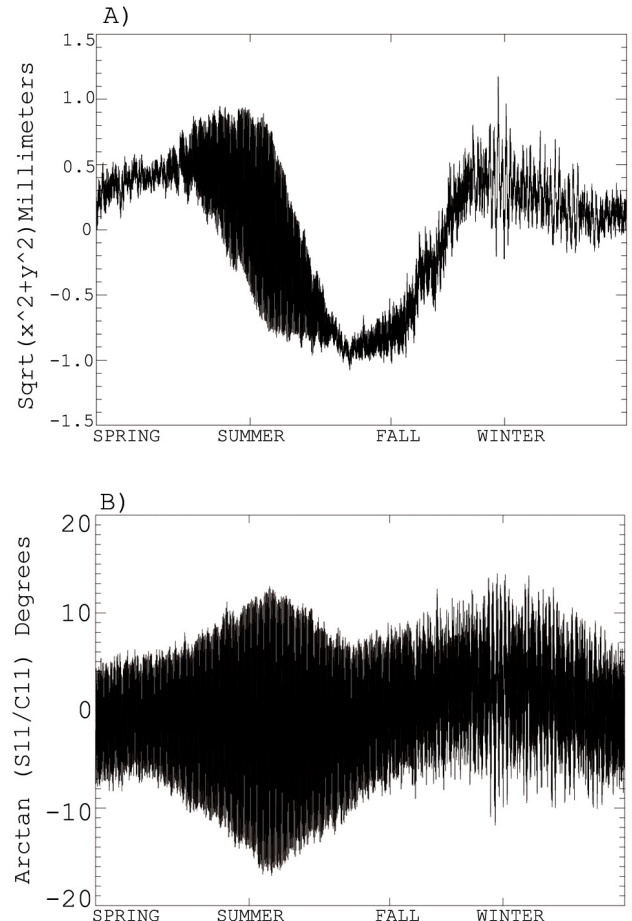
**Figure 12.** Equatorial displacement of center of mass. (a) $V_{cm} = R(\Delta C_{11}^2 + \Delta S_{11}^2)^{1/2}$. (b) $\Phi_{cm} = \arctan(\Delta S_{11}/\Delta C_{11})$.

Table 8. Comparison of Tracking Data Analysis Results of *Yoder et al.* [2003] and Model Results From This Investigation^a

Zonal Coefficient	Main Harmonics, Cycles per Year (Amplitude, 10^{-9})		
	This Investigation	<i>Yoder et al.</i> [2003]	Error bounds [<i>Yoder et al.</i> , 2003]
ΔC_{20}	1 (0.88)	1 (1.81)	1.02
	2 (0.92)	2 (2.32)	0.94
	3 (0.23)		
	4 (0.12)		
ΔC_{30}	1 (2.53)	1 (6.59)	0.28
	2 (0.22)	2 (1.34)	0.26
	3 (0.29)	3 (0.25)	0.24
	4 (0.09)	4 (0.43)	0.22

^aAmplitude and frequency of main harmonics for second and third degree zonals.

five daily harmonics with periods between 0.997 and 1.003 days with amplitudes ranging between 0.046 and 0.068 mm.

[60] The main daily harmonic in the time series for the phase angle (Φ_{cm}) has amplitude of 3.94° , an annual harmonic follows with 0.93° amplitude. Four daily harmonics with periods between 0.998 and 1.001 days show amplitudes in the 0.83° – 0.49° range. A semiannual harmonic has amplitude of 0.42° .

[61] The magnitude V_{cm} oscillates about a permanent value of 4.78 mm, with a maximum variation of 1.17 mm and a minimum of -1.07 mm. The maximum occurs at 506 sols, the minimum at 319 sols. The phase Φ_{cm} oscillates about a permanent value of 84.2° . The oscillation in Φ_{cm} reaches a maximum of 14.0° at 507 sols, the minimum of -16.9° occurs at 222 sols.

5. Comparison to Previous Investigations

[62] *Karatekin et al.* [2005] display graphical results for the variations in the zonal coefficients of degrees 2 to 5 based on outputs from the NASA Ames GCM as well as those from the LMD GCM [*Forget et al.*, 1999] and those based on data from the High Energy Neutron Detector (HEND) instrument on board the Mars Odyssey spacecraft. Their results for the NASA Ames GCM are given in different units but the graphical similarity to our results is clearly evident.

[63] The results of *Karatekin et al.* [2005] indicate that the existing tracking data solutions can not discriminate between the Stokes coefficients produced by existing atmospheric models or by HEND data. Nevertheless, some results of this investigation can be compared to results appearing in the literature.

[64] *Yoder et al.* [2003] investigated the seasonal changes in zonal gravity coefficients, which arise from the variations in ice cap growth and decay. They analyzed MGS radio tracking data to estimate variations in the second and third degree zonals. Their results are given in Table 8; the results of this investigation are shown as well. The values estimated by *Yoder et al.* [2003] are larger than those of this investigation, with the exception of the (1/3)-annual harmonic for ΔC_{30} . The large values for the estimation errors (column three) have to be considered. Other details of the estimation procedure are not clear. It is possible that their results incorporate the effects of higher-degree zonals.

[65] *Yoder et al.* [2003] explored the influence of ice-cap mass distributions with the use of four different ice thickness profiles as a function of latitude. The models are as follows: Model A: uniform thickness to colatitude 35° ; Model B, thickness decreasing with colatitude θ , proportional to $(35^\circ - \theta)^{1/2}$; Model B*, as B with south cap boundary extended to 40° ; and Model C, thickness proportional to $(35^\circ - \theta)$.

[66] They computed the predicted amplitude of the changes in zonal gravity coefficients relative to the leading term for the four ice-cap mass distributions. Their results as well as the corresponding values from this investigation are given in Table 9. The results shown for this investigation include the even zonals from 2 to 12 and the odd zonals from 3 to 13. If the annual variation for the even zonals is extended to degree 40, the ratio to the first term (first column) reaches a value of 2.21.

[67] It is not clear from their paper if the results of *Yoder et al.* [2003] for the four ice thickness models refer to the annual time harmonic. If so, their results for model (C) are closest to ours. Comparison of Figure 4 in their paper with our Figure 3 indicates that ice thickness distribution (Model C) is the one with greatest similarity.

[68] *Van Hoolst et al.* [2002] computed seasonal variations in the position of the center of mass by using the LMD atmospheric GCM. They found an annual cycle equatorial effect smaller than 1 mm and a motion along the rotation axis at the same frequency with a peak-to-peak amplitude of 6.5 cm. This investigation obtains equatorial displacement amplitudes of 0.25 mm (annual), 0.19 mm (semiannual) and 0.04 mm (1/3-annual). A number of very closely grouped daily harmonics add up to more than 0.30 mm amplitude. The displacement along the z axis exhibits an annual harmonic with 12.7 mm amplitude. The peak-to-peak displacement (all frequencies included) is 49.8 mm. The LMD model used by *Van Hoolst et al.* [2002] and the NASA/Ames GCM used in this investigation do not have identical rates of CO_2 condensation and sublimation. There is a difference in sampling rates between the two investigations. *Van Hoolst et al.* [2002] used seasonal mean values of surface pressure and ice cap loading mass data; these averages are based on simulations, which include time steps of approximately 2 hours. This

Table 9. Comparison of Results of *Yoder et al.* [2003] and This Investigation^a

Model	Variation in Even Zonals/Variation in C20	Variation in Odd Zonals/Variation in C30	$\Delta C_{50}/\Delta C_{30}$
<i>Yoder et al.</i> [2003]			
A	1.26	0.96	0.22
<i>Yoder et al.</i> [2003]			
B*	1.54	1.24	0.29
<i>Yoder et al.</i> [2003]			
B	1.98	1.32	0.44
<i>Yoder et al.</i> [2003]			
C	2.66	1.74	0.56
This investigation			
Annual	1.74	1.76	0.50
(1/2)-annual	2.47	2.82	0.69
(1/3)-annual	2.58	3.43	0.91

^aRatio of variations in even and odd zonals to the leading term, and ratio of fifth to third degree zonal for various ice caps thickness models.

t1.1 **Table 10.** Orbit Perturbations in Mars Global Surveyor Orbiter Caused By Variations in Mars' Gravitational Field Due to Changes in the Ice Caps and Changes in Atmospheric Mass Distribution^a

t1.2	Season	Direct Effect RMS, m	Effect After Adjustment RMS, m
t1.3	Spring	4.44	0.35
t1.4	Summer	17.37	0.74
t1.5	Fall	13.63	0.61
t1.6	Winter	17.39	0.78

^aResults for four 7-day arcs at the beginning of each of the Martian seasons. The gravitational field variations were represented by a full spherical harmonic expansion to degree and order 40.

t1.7

investigation uses data points spaced at 1.5 Martian hours (16 points per sol).

6. Mars Global Surveyor Orbit Perturbation

[69] The GEODYN orbit determination and geodetic parameter estimation software [Putney, 1977] was used to gauge the size of perturbations in the Mars Global Surveyor (MGS) orbit caused by variations in Mars' gravitational field due to changes in the ice caps as well as changes in the atmospheric mass distribution.

[70] The gravitational field variations were represented by a full spherical harmonic expansion to degree and order 40, with a time interval of 1.5 Martian hours. The coefficients in this series represent the difference in mass distribution with respect to a mean gravity field GMM-2B [Lemoine *et al.*, 2001]. GEODYN is able to ingest such a time series of "delta" coefficients and apply them in orbit computations.

[71] To gauge the orbit perturbations on MGS caused by seasonal mass redistribution and other atmospheric effects, a 7-day "truth" trajectory was generated. The truth trajectory did not use the time series of delta coefficients. A second trajectory was then generated using the time series of delta coefficients. The computation of this trajectory was identical in all respects to the first, with the exception of the use of the delta coefficients. This procedure was performed at four 7-day time intervals at the beginning of each of the Martian seasons. The results are listed in Table 10.

[72] In practice, orbit perturbations are observed in trajectories that have been determined with tracking data in least squares solutions. In such trajectories some level of a perturbation is absorbed into initial state parameters as well as other estimated parameters. Therefore we attempted to gauge how much of the ice caps variations and atmospheric mass redistribution would be observed in a trajectory that had been determined from tracking data. In this case the truth trajectory was used as a proxy for tracking data. Four orbit solutions over seven days at the beginning of each season were performed using the truth trajectory as data. The time series of gravity coefficients were used in the force model of the orbit solution (the truth trajectory was generated without the time series). The trajectory generated by the orbit solution was then compared to the truth trajectory. The results appear in Table 10 also.

[73] The perturbations in position shown in Table 10 are in the neighborhood of the limit at which they can be detected with state of the art orbit determination capabilities.

Note the larger perturbations associated with the summer and winter epochs, which correspond to the times when the ice caps are experiencing largest variations.

7. Summary and Conclusions

[74] Outputs from the NASA/Ames Mars GCM have been used to compute time variations of the Stokes coefficients, which appear in a spherical harmonic expansion of Mars' gravitational field. The resulting time series cover a period equal to the length of the Martian year (669 sols), with a time step of 1.5 hours.

[75] The gravitational field variations were divided into those produced by the variations of the Martian ice caps and those due to mass variations of the atmosphere. For presentation purposes the variations were separated in two sets. The first set consisted of the zonal variations while the second set was composed of the sectorial and tesseral variations. The time series expressing the variations of the coefficients were analyzed by means of Fast Fourier transform techniques. The results indicate that the zonal variations are produced mainly by the variations in the polar ice caps. This is true for the total power over all frequencies as well as for the main harmonics. In general, the main harmonics are annual, (1/2)-annual and (1/3)-annual.

[76] The zonal variations were analyzed in terms of the separate contributions due to the northern and southern ice caps. It was determined that even time harmonics are in/out of phase for the even/odd degree zonal variations and that odd time harmonics are in/out of phase for the odd/even degree zonal variations.

[77] Analysis of the sectorial and tesseral variations indicates that atmospheric contributions are larger in terms of total power. The results are more complex when expressed in terms of main harmonics. The ΔC_{11} variation is due mainly to a daily harmonic produced by the atmosphere. Other variations show main annual and (1/2)-annual harmonics with atmospheric and ice contributions of similar magnitudes. When daily or (1/2)-daily main harmonics appear, they are entirely due to the atmosphere. The sectorial variations ΔC_{22} and ΔS_{22} exhibit annual, (1/2)-annual and (1/2)-daily main harmonics that are mostly due to the atmosphere. The sectorial and tesseral variations due to ice caps are produced by their asymmetrical configuration. The atmospheric contributions are associated with asymmetries in surface topography [Van den Acker *et al.*, 2002]. The complex interactions of the atmosphere with the topography can produce a rich spectrum of responses [Read and Lewis, 2004].

[78] With respect to the results in the time domain it is clear that long period harmonics are associated with seasonal effects, involving the revolution of Mars around the Sun and the inclination of its rotation axis with respect to the plane of the orbit. Daily and subdaily periods are associated with the daily rotational motion.

[79] A full 40-degree and order set of coefficient variations was used to generate orbital perturbations of the Mars Global Surveyor spacecraft. Four 7-day orbit solutions were performed at the beginning of each season. The perturbations in position shown in Table 10 are in the neighborhood of the limit at which they can be detected with state of the art orbit determination capabilities. The largest perturba-

tions were associated with the summer and winter epochs, which correspond to the times when the ice caps are experiencing largest variations. Future efforts should include the estimation of velocity components for which there exists greater precision in present-day systems. The estimation should be extended to arcs of longer duration since the results indicate that the larger variations have main time harmonics with seasonal periodicities.

[80] At the present time, the tracking data from Mars' orbiters does not allow to discriminate between the pattern of CO₂ sublimation and condensation available from different Mars atmospheric models. Simulations by *Karatekin et al.* [2005] indicate the importance of incorporating higher-degree zonals with respect to the possibility of extracting information about atmospheric air/ice dynamics from the time variation of Mars' gravitational coefficients. The results of this investigation provide some insight on the nominal behavior of the higher degree coefficients, which could be incorporated in future space geodesy efforts.

[81] To the extent that these variations of Mars' gravity field can be detected, they will provide a measure of the processes taking place in Mars' ice caps and atmosphere and might allow to discriminate among various atmospheric models. Furthermore, as the time variable gravity field becomes more accurate, the tracking of orbiting spacecraft will improve accordingly.

[82] **Acknowledgments.** We are grateful to the anonymous reviewers for their reading of the paper and their constructive remarks. We are grateful to Herbert V. Frey for providing encouragement and support as chief of the Planetary Geodynamics Laboratory. We are thankful to Terry Sabaka of RITSS for developing the MATLAB software used in the harmonic analysis. We are thankful to James Schaeffer at NASA Ames Research Center for providing the data from the NASA/Ames Mars GCM.

References

- Byrne, S., and A. P. Ingersoll (2003), A sublimation model for Martian South Polar ice features, *Science*, *299*, 1051–1053.
- Caputo, M. (1967), *The Gravity Field of the Earth*, Elsevier, New York.
- Chao, B. F., and D. P. Rubincam (1990), Variations of Mars gravitational field and rotation due to seasonal CO₂ exchange, *J. Geophys. Res.*, *95*(B9), 14,755–14,760.
- Defraigne, P., O. de Viron, V. Dehant, T. Van Hoolst, and F. Hourdin (2000), Mars rotation variations induced by atmosphere and ice caps, *J. Geophys. Res.*, *105*(E10), 24,563–24,570.
- Forget, F., F. Hourdin, R. Fournier, C. Hourdin, O. Talagrand, M. Collins, S. R. Lewis, P. L. Read, and J. P. Huot (1999), Improved general circulation models of the Martian atmosphere from the surface to above 80 km, *J. Geophys. Res.*, *104*(E10), 24,155–24,175.
- Hamming, R. W. (1986), *Numerical Methods for Scientists and Engineers*, 2nd ed., Dover, Mineola, New York.
- Hartmann, W. K. (1993), *Moons and Planets*, Wadsworth, Stamford, Conn.
- Karatekin, Ö., J. Duron, P. Rosenblatt, T. Van Hoolst, and V. Dehant (2005), Mars' time-variable gravity and its determination: Simulated geodesy experiments, *J. Geophys. Res.*, *110*, E06001, doi:10.1029/2004JE002378.
- Kieffer, H. H., B. M. Jakosky, C. W. Snyder, and M. S. Matthews (Eds.) (1992), *Mars*, Univ. of Ariz. Press, Tucson.
- Lambeck, K. (1988), *Geophysical Geodesy: The Slow Deformations of the Earth*, Clarendon, Oxford, U. K.
- Lemoine, F. G., D. E. Smith, D. D. Rowlands, M. T. Zuber, G. A. Neumann, D. S. Chinn, and D. E. Pavlis (2001), An improved solution of the gravity field of Mars (GMM-2b) from Mars Global Surveyor, *J. Geophys. Res.*, *106*(E10), 23,359–23,376.
- Putney, B. H. (1977), General theory for dynamic satellite geodesy, in *The National Geodetic Satellite Program, NASA Spec. Publ., SP-365*, 319–334.
- Read, P. L., and S. R. Lewis (2004), *The Martian Climate Revisited*, Springer, New York.
- Sanchez, B. V., D. D. Rowlands, R. M. Haberle, and J. Schaeffer (2003), Atmospheric rotational effects on Mars based on the NASA Ames general circulation model, *J. Geophys. Res.*, *108*(E5), 5040, doi:10.1029/2002JE001984.
- Sanchez, B. V., R. M. Haberle, and J. Schaeffer (2004), Atmospheric rotational effects on Mars based on the NASA Ames general circulation model: Angular momentum approach, *J. Geophys. Res.*, *109*, E08005, doi:10.1029/2004JE002254.
- Smith, D. E., and M. T. Zuber (1996), The shape of Mars and the topographic signature of the hemispheric dichotomy, *Science*, *271*, 184–188.
- Smith, D. E., M. T. Zuber, R. M. Haberle, D. D. Rowlands, and J. R. Murphy (1999), The Mars seasonal CO₂ cycle and the time variation of the gravity field: A general circulation model simulation, *J. Geophys. Res.*, *104*(E1), 1885–1896.
- Smith, D. E., et al. (2001), Mars Orbiter Laser Altimeter: Experiment summary after the first year of global mapping of Mars, *J. Geophys. Res.*, *106*(E10), 23,689–23,722.
- Van den Acker, E., T. Van Hoolst, O. de Viron, P. Defraigne, F. Forget, F. Hourdin, and V. Dehant (2002), Influence of the seasonal winds and the CO₂ mass exchange between atmosphere and polar caps on Mars' rotation, *J. Geophys. Res.*, *107*(E7), 5055, doi:10.1029/2000JE001539.
- Van Hoolst, T., V. Dehant, O. de Viron, P. Defraigne, and J.-P. Barriot (2002), Degree-one displacement on Mars, *Geophys. Res. Lett.*, *29*(11), 1511, doi:10.1029/2002GL014711.
- Yoder, C. F., A. S. Konopliv, D. N. Yuan, E. M. Standish, and W. M. Folkner (2003), Fluid core size of Mars from detection of the solar tide, *Science*, *300*, 299–303.

R. M. Haberle, Space Sciences Division, NASA Ames Research Center, Moffett Field, CA 94035, USA. (robert.m.haberle@nasa.gov)

D. D. Rowlands, Space Geodesy Laboratory, NASA Goddard Space Flight Center, Greenbelt, MD 20771, USA. (david.d.rowlands@nasa.gov)

B. V. Sanchez, Planetary Geodynamics Laboratory, NASA Goddard Space Flight Center, Greenbelt, MD 20771, USA. (braulio.v.sanchez@nasa.gov)